Supporting Information

Hierarchical porous structures with heterogeneous interfaces in CoC@(C/rGO) nanocomposites for broadband electromagnetic wave absorption

Xiaonan Guo[a,#], Youwei Zhang[b,#], Fan Jiang[c], Wei Liu[a], Xuan Bai[a], Zeyu Zhang[c], Jiuxin Li[a], Chen Chen[a], Jing Peng[c], Xiuqin Zhang[a], Huiling Ma[a,*], Maolin Zhai[c,*]

[a] *Beijing Key Laboratory of Clothing Materials R&D and Assessment, Beijing Engineering Research Center of Textile Nanofiber, School of Materials Science & Engineering, Beijing Institute of Fashion Technology, Beijing 100029, China*

[b] *Beijing Institute of Aeronautical Materials, Beijing 100095, China*

[c] *Beijing National Laboratory for Molecular Sciences, Department of Applied Chemistry and the Key Laboratory of Polymer Chemistry and Physics of the Ministry of Education, College of Chemistry and Molecular Engineering, Peking University, Beijing 100871, China*

[*]Corresponding authors. E-mail address: hlma@bift.edu.cn; mlzhai@pku.edu.cn

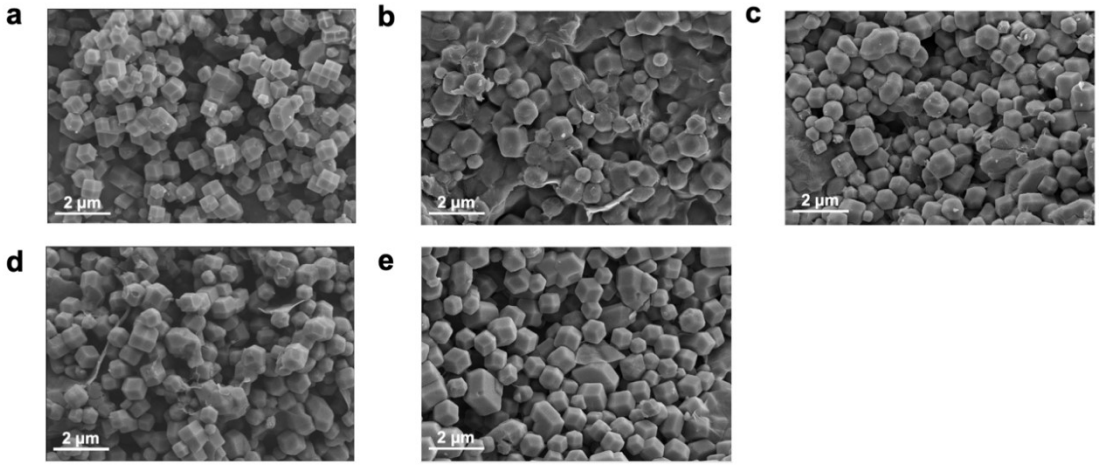

Fig. S1. SEM images of (a) ZIF-67, (b) ZIF-67@(CNF/GO)-I, (c) ZIF-67@(CNF/GO)-II, (d) ZIF-67@(CNF/GO)-III, and (e) ZIF-67@(CNF/GO)-IV.

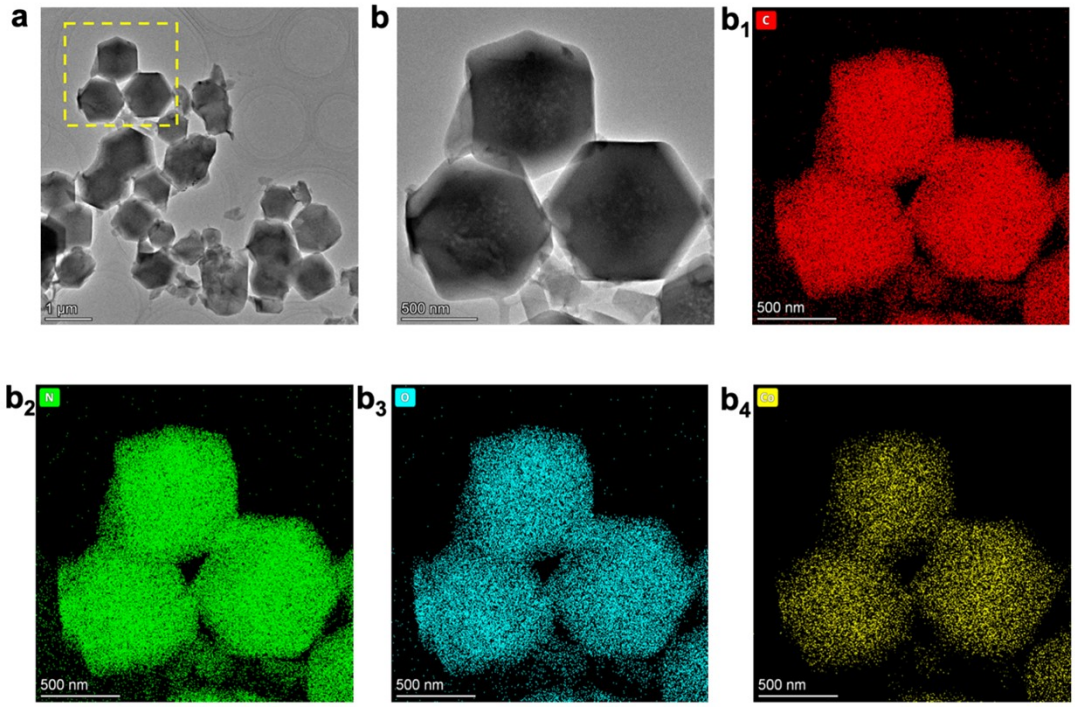

Fig. S2. TEM images of (a-b) ZIF-67@(CNF/GO)-III.

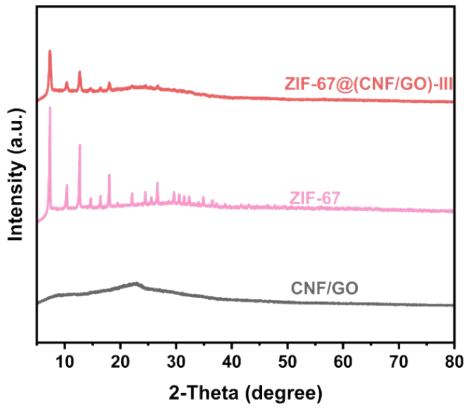

Fig. S3. XRD patterns of ZIF-67, CNF/GO, and ZIF-67@(CNF/GO)-III.

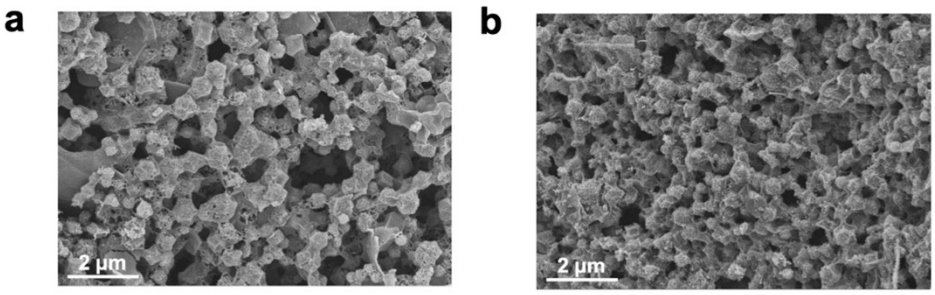

Fig. S4. SEM images of (a) CoC@(C/rGO)-III-500, and (b) CoC@(C/rGO)-III-700.

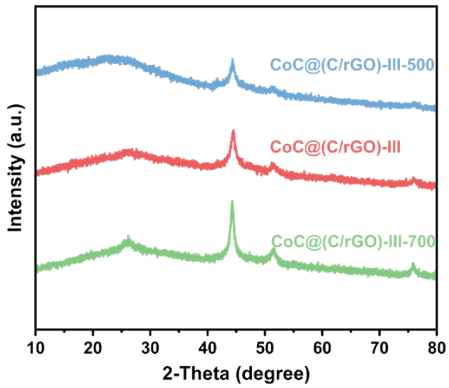

Fig. S5. XRD patterns of CoC@(C/rGO)-III-500, CoC@(C/rGO)-III and CoC@(C/rGO)-III-700.

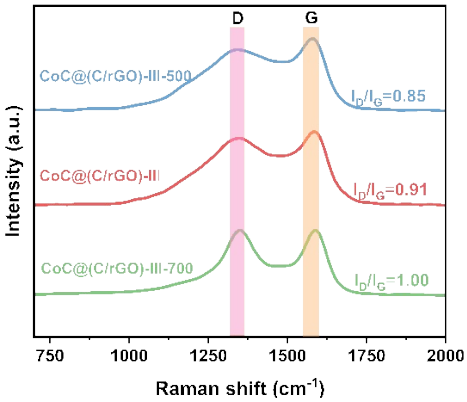

Fig. S6. Raman spectra of CoC@(C/rGO)-III-500, CoC@(C/rGO)-III, and CoC@(C/rGO)-III-700.

Table S1. BET surface area analysis of CoC, C/rGO, and CoC@(C/rGO)-X (labeled I-IV).

	SSA（m^2/g）	Pore volume（cm^3/g）	Average pore size（nm）
C/rGO	1.3	0.002	34.6
CoC@(C/rGO)-I	3.9	0.024	32.1
CoC@(C/rGO)-II	13.2	0.077	23.3
CoC@(C/rGO)-III	68.4	0.200	12.5
CoC@(C/rGO)-IV	35.2	0.082	13.8
CoC	396.6	0.150	0.6

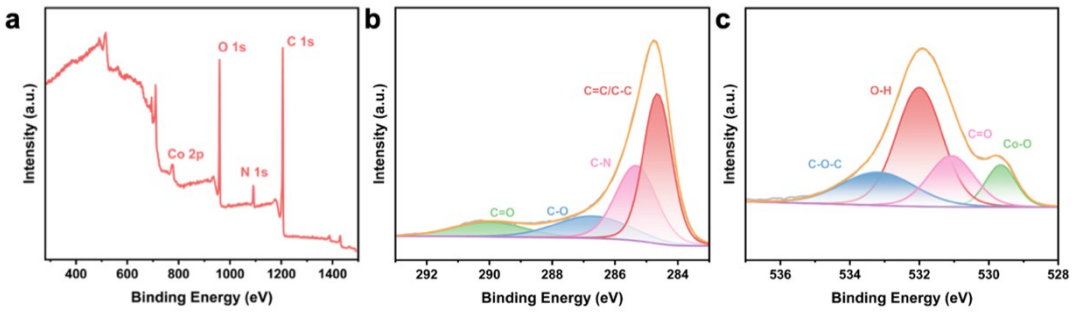

Fig. S7. XPS patterns of CoC@(C/rGO)-III (a) survey scan, (b) C 1s, and (c) O 1s.

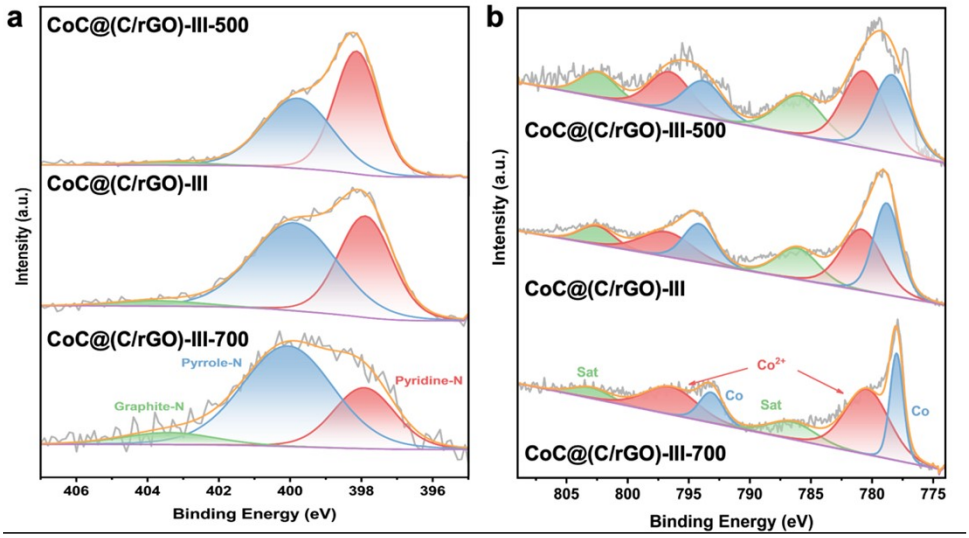

Fig. S8. XPS spectra of CoC@(C/rGO)-III-500, CoC@(C/rGO)-III, and CoC@(C/rGO)-III-700: (a) N 1s, and (b) Co 2p.

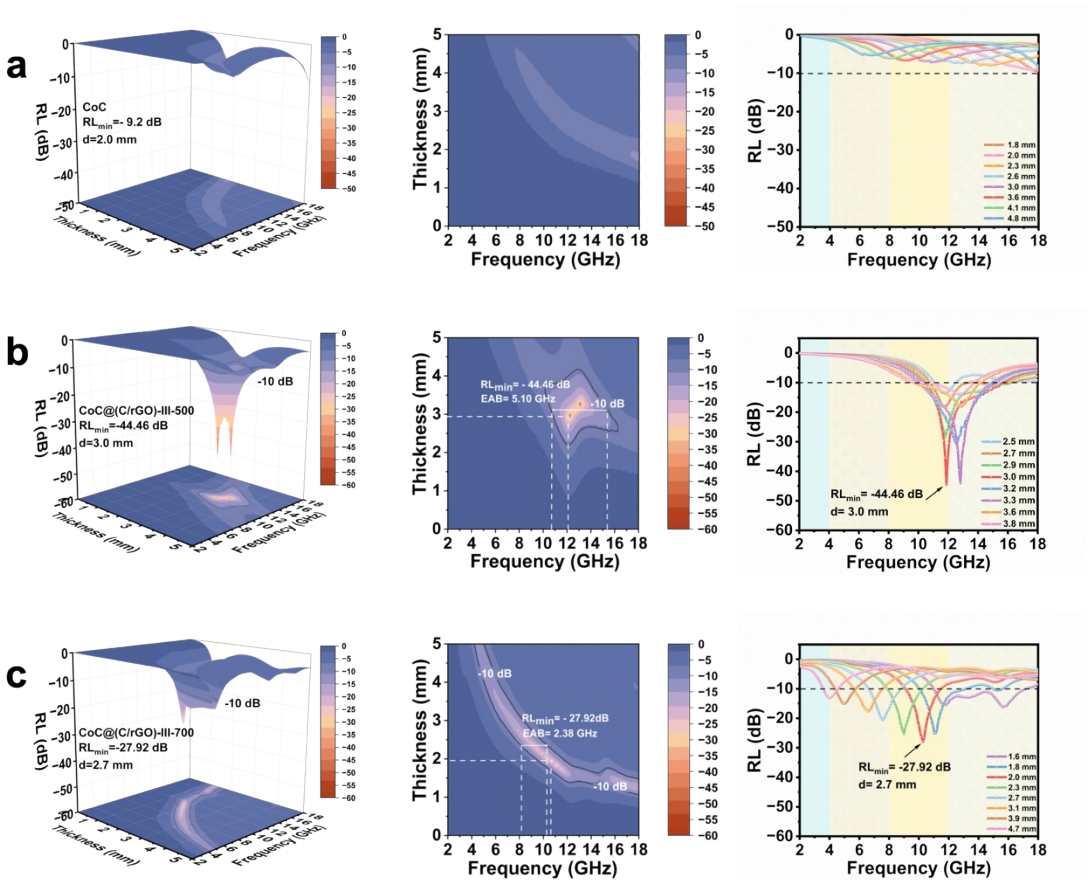

Fig. S9. The 3D representations, 2D projection images and RL values with different thicknesses of (a) CoC, (b) CoC@(C/rGO)-III-500, and (c) CoC@(C/rGO)-III-700.

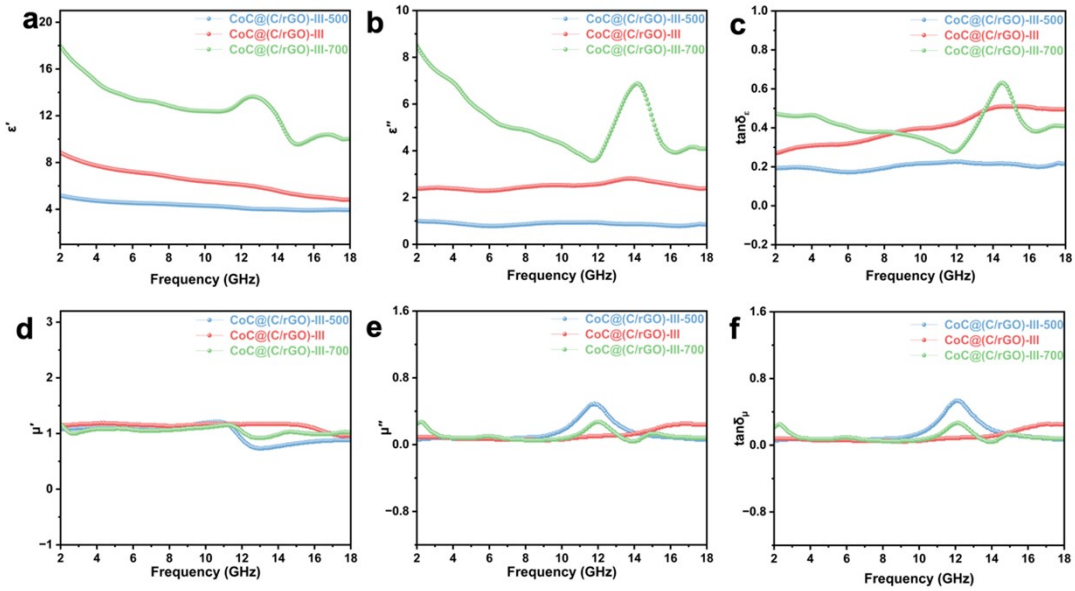

Fig. S10. (a) ε′, (b) ε" and (c) $\tan\delta_{\varepsilon}$, (d) μ′, (e) μ", and (f) $\tan\delta_{\mu}$ of CoC@(C/rGO)-III-500, CoC@(C/rGO)-III, and CoC@(C/rGO)-III-700.

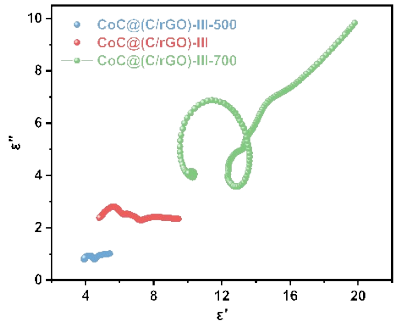

Fig. S11. Cole-Cole curves of CoC@(C/rGO)-III-500, CoC@(C/rGO)-III and CoC@(C/rGO)-III-700.

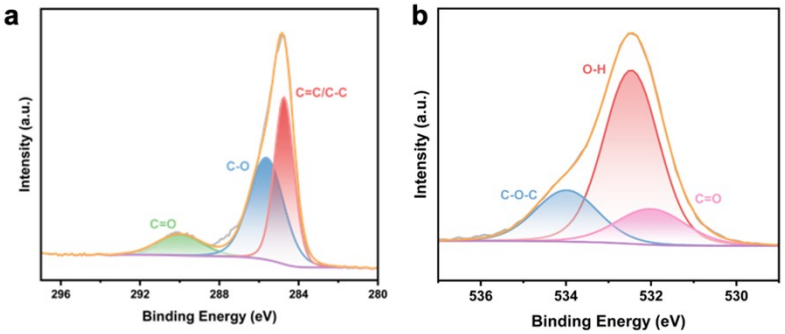

Fig. S12. XPS spectra of C (a) C 1s and (b) O 1s.

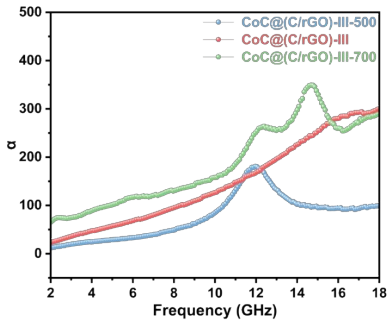

Fig. S13. attenuation constant of CoC@(C/rGO)-III-500, CoC@(C/rGO)-III, and CoC@(C/rGO)-III-700.

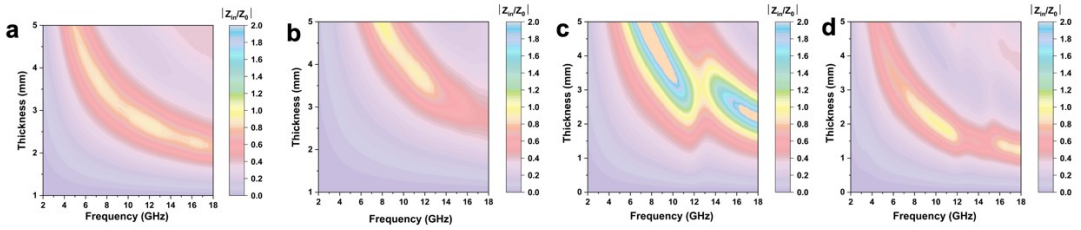

Fig. S14. 2D impedance matching curves of (a) CoC@(C/rGO)-I, (b) CoC@(C/rGO)-II，(c) CoC@(C/rGO)-III-500, and (d) CoC@(C/rGO)-III-700.

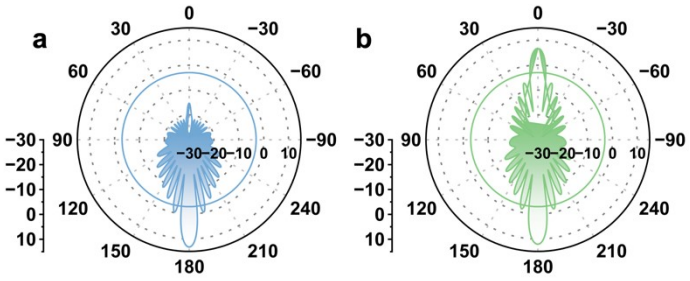

Fig. S15. 2D RCS simulation results of (a) CoC@(C/rGO)-III-500 and (b) CoC@(C/rGO)-III-700.